The Composites 2024 International Conference

March 06 to 08 2024, Seville, Spain

Conference Proceedings

DOI:
https://doi.org/10.26799/cp-composites-2024

Proceedings of the Composites 2024 International Conference
Seville, Spain – March 06 – 08, 2024
DOI: : https://doi.org/10.26799/cp-composites-2024

A New Optical Method for Surface Quality Analyses of Thermoplastic Composite Parts

J. Birtha [1,*], E. Kobler [1], C. Marschik[1], K. Straka [2], G. Steinbichler [2]

[1] Competence Center CHASE GmbH, Hafenstraße 47-51, Linz, Austria, janos.birtha@chasecenter.at
[2] Johannes Kepler University Linz, Institute of Polymer Injection Molding and Process Automation Altenberger Straße 69, 4040 Linz, Austria

Abstract

During the processing of fiber-reinforced thermoplastic composites, surface defects such as in-plane fiber waviness and surface grooves can occur. These defects have a detrimental effect on the surface quality and mechanical performance of components. Quantifying the surface quality requires adequate measurement systems, which moreover help to investigate the relationship between processing parameters and critical quality attributes and ultimately optimize process conditions. We propose an optical measurement approach based on a monochrome line scan camera to analyze the surface of flat composite parts. The camera is mounted on a rail and moves horizontally at a constant speed over a fixed distance while scanning the subjacent component. The recorded images are analyzed using OrientationJ, a plugin for an image analysis software (ImageJ®), which can analyze the gradient tensor in a local neighborhood. In addition, the tool can be used to measure orientation and Isotropy properties of an image, including (i) standard deviation of orientation, which assesses fiber orientation variation, (ii) coherency, which determines the presence of a dominant direction in the local structure, (iii) and gradient energy, which measures region homogeneity. Using these metrics, we performed measurements of surface quality in various thermoplastic composite plates, including a polycarbonate/carbon fiber (PC/CF) plate, a PC/CF plate consolidated with a polyetherimide (PEI) foil, and a polyaryletherketone (PAEK) plate. Our study shows that the new measurement system can quantitatively assess surface defects and fiber waviness in thermoplastic composite plates in a non-destructive, quick, and effective manner.

Keywords: Thermoplastic composites, surface quality, fiber waviness, optical measurement system, surface defects, OrientationJ

1. Introduction

Thermoplastic composites are prominent candidates for lightweight design, offering good specific strength, recyclability, and excellent vibration damping capabilities [1,2]. In our prior research, we demonstrated how UD tapes can be fabricated to composite plates by using a heating and cooling press in combination [3]. This setup involves a two-step process: initially, the UD tapes are bonded together in the heating press, where the major amount of air between the individual tapes is eliminated. Subsequently, two steel carrier tools transfer the bonded tape stack to the cooling press, where the material is cooled down while voids are eliminated by applying pressure. Challenges, especially during cooling, persist in the manufacturing process, as defects like delamination, surface defects, or fiber breakage may arise [4]. This study focuses on two surface defects: (i) fiber waviness and (ii) surface grooves. The former mainly occurs during the shrinkage of the tools due to cooling during the process, which imposes an axial force onto the laminate, causing the fibers to buckle. Further details on this phenomenon were provided by Krämer [5]. The latter is caused by degradation effects and/or voids that diffuse between tool and laminate, remaining trapped within the grooves of the tool. These defects compromise both the mechanical and optical properties of composites parts; and as a result, there is a need to measure them in a fast and non-destructive manner.
We have developed a new non-destructive optical measurement approach to assess the fiber orientation and defects on the surface of thermoplastic composite laminates. In this work, we investigate its ability to analyze different thermoplastic composite materials, including a polycarbonate/carbon fiber (PC/CF) plate, a PC/CF plate consolidated with a polyetherimide (PEI) foil on the top to improve surface quality, and a polyaryletherketone/carbon fiber (PAEK/CF) plate. The recorded images were further analyzed by means of a Python script and OrientationJ, a plugin within the software ImageJ ®, to derive objective quality metrics that allow a ranking of the different surface qualities.

DOI: : https://doi.org/10.26799/cp-composites-2024

2. Experimental

We investigated three different thermoplastic composite plates. Specifically, we analyzed the surface quality of two consolidated PC/CF tape-stacks, one of which was consolidated with a PEI layer placed on the top of the stack. Additionally, a consolidated PAEK/CF tape-stack was included in the analysis. For consolidation, we utilized the consolidation unit from FILL GmbH [3]. A so-called Photobox was developed to investigate the surface quality of various thermoplastic composite parts, that consists of four main features (see Figure 1).

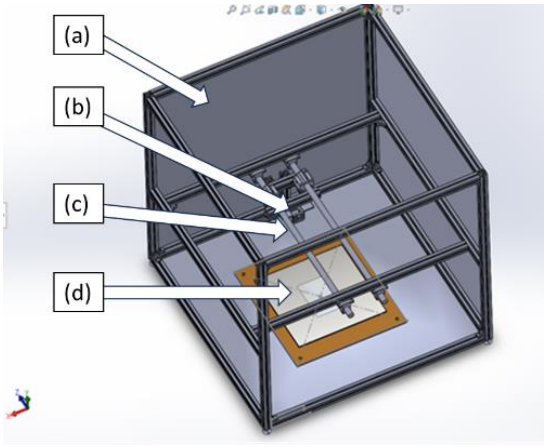

Fig 1.: Schematic representation of the Photobox: (a) 1 x 1 x 1 m sized closed black box, (b) linescan camera, (c) horizontal movement system, (d) 6 mm thick non-reflective glass.

The measurement system is enclosed within a 1 x 1 x 1 m black box to prevent external light from affecting the setup (see Figure 1 (a)). Imaging is performed using a NECTA N4K-3-C monochrome linescan camera with a resolution of 4096 x 1 and a pixel size of 3.5 x 3.5 µm (see Figure 1 (b)). The camera is equipped with a Basler C11-3520-12M-P-2200000578 1.1" lens, which allows for a minimum working distance of 150 mm. To guarantee constant light conditions, an LED light strip at an angle of 30° is attached to the camera. To facilitate scanning across surfaces, a horizontal movement system was implemented, ensuring synchronized movement of the camera and the light strip (see Figure 1 (c)). Finally, a 6 mm thick non-reflective glass is placed on top of the composite plates to fix them in position (see Figure 1 (d)). A Python script was developed to merge the pictures of each linescan into a complete image of the composite plate.

Due to the robustness of the components, no vibrations occur during camera movement. Moreover, the synchronous movement of the camera and light strip ensures uniform light conditions with consistent intensity. Finally, it is possible to achieve a resolution of approximately 24 µm/pixel, allowing for detailed measurements and observations.

The optical pictures were analyzed using the OrientationJ plugin within the ImageJ software. The aim was to characterize the orientation and isotropy of a local region of interest (ROI) using a gradient tensor. A detailed description of the methodology was given by Püspöki et al. [6]. In this study, we utilized a 3-pixel wide region of interest with a Gaussian gradient tensor to analyze our pictures. To evaluate the surface quality of the fabricated plates, three different metrics were employed. First, the standard deviation of orientation was used to assess the fiber waviness on the plate surfaces. A higher deviation indicates more waviness, as the fiber orientation changes more frequently within the ROI. Second, the coherency of the fiber orientation was evaluated: a coherency value of 1 indicates that the local structure has one defined orientation, while a value of 0 suggests that the fibers are ramdomly oriented. Third, a gradient energy was calculated. Preliminary investigations suggested that an energy value closer to 0 indicates fewer surface grooves.

3. Results and discussion

Figure 2 shows the optical pictures of (i) a PC/CF plate (Figure 2(a)), (ii) a PC/CF plate consolidated with a PEI foil (Figure 2(b)), and (iii) both the top (Figure 2(c)) and bottom (Figure 2(d)) halves of a PAEK/CF plate. Table 1 displays the results from the analysis conducted using OrientationJ. Observing the consolidation of PC/CF plates, the use of a PEI layer on the top surface leads to reduced fiber waviness (indicated by a lower standard deviation of orientation and higher mean coherency) and fewer surface grooves (shown by a lower

DOI: : https://doi.org/10.26799/cp-composites-2024

mean energy). This improvement in surface quality can primarily be attributed to the thermal stability and smooth surface of the PEI foil. The stability results in less axial force imposed onto the composite plate, while the smooth surface aids in reducing surface grooves, thereby enhancing overall quality. Moreover, the ability to select different regions of interest (ROIs) allows for spatial analysis. Figures 2(c) and (d) demonstrate that the fiber orientation on the top section of the PAEK/CF plate is mostly straight, whereas the bottom section exhibits much higher fiber waviness. Quantitatively, both the standard deviation of fiber orientation and mean coherency support this observation. This indicates that more fibers buckled under the axial forces during cooling, suggesting either higher cooling rates or better contact between the part and the consolidation tool.

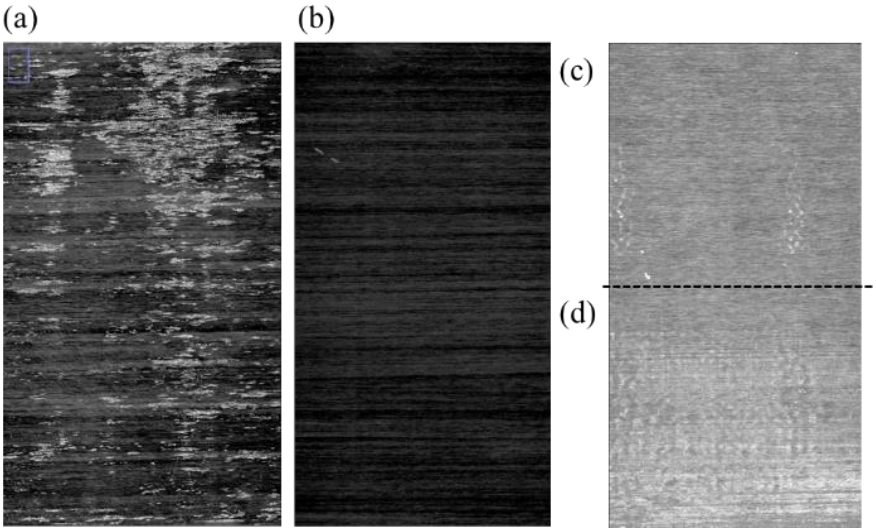

Fig. 2.: Optical pictures of (a) PC/CF plate, (b) PC/CF plate consolidated with a PEI foil, (c) top and (d) bottom half of a PAEK/CF plate.

Table 1. Results from the analysis from OrientationJ of the composite plates under investigation.

Plate	St.Dev. of Fiber orientation [°]	Mean Coherency [-]	Mean Energy [-]
PC/CF	7.073	0.678	0.092
PC/CF + PEI	5.399	0.7	0.025
Top of PAEK/CF	2.382	0.851	0.11
Bottom of PAEK/CF	6.738	0.634	0.107

4. Conclusion

The primary objectives of the newly developed measurement system were to ensure that it is (i) user-independent, (ii) reproducible, (iii) quantitative, and (iv) capable of providing fast (<10 minutes) assessments over a large surface area (500 x 500 mm). Our study has showcased the effectiveness of utilizing an optical linescan camera alongside OrientationJ for the quantitative and objective assessment of surface quality in thermoplastic composite plates. The approach enables fast and efficient measurements, thus paving the way for process optimization in this area. Future investigations will focus on composite plates with varied surface finishes to explore the broader applicability of our measurement system.

Acknowledgements

This work was performed within the Competence Center CHASE GmbH, funded by the Austrian Research and Promotion Agency. The authors acknowledge financial support by the COMET Centre CHASE, which is funded within the framework of COMET—Competence Centers for Excellent Technologies—by BMVIT, BMDW, and the Federal Provinces of Upper Austria and Vienna. The COMET program is run by the Austrian Research Promotion Agency (FFG).

References

1. J. Njuguna, “Lightweight Composite Structures in Transport :Design, Manufacturing, Analysis and Performance”; Elsevier: Amsterdam, The Netherlands, 2016; ISBN 978-1-78242-343-0.

DOI: : https://doi.org/10.26799/cp-composites-2024

2. M. Biron, "Thermosets and Composites: Material Selection, Applications, Manufacturing, and Cost Analysis", 2nd ed.; Elsevier: Amsterdam, The Netherlands, 2013.
3. J. Birtha, E. Kobler, C. Marschik, K. Straka, G. Steinbichler, "Using Heating and Cooling Presses in Combination to Optimize the Consolidation Process of Polycarbonate-Based Unidirectional Thermoplastic Composite Tapes", Polymers, vol 15 (23), MDPI, 2023.
4. M. Wenninger, "A Novel Measurement Approach for the Inline Quality Assessment of Thermoplastic, Glass-Fiber-Reinforced, Unidirectional Tapes Based on Optical Coherence Tomography", Ph.D. dissertation, Johannes Kepler Universität, Linz.
5. E.T.M. Krämer, "The formation of fiber waviness during thermoplastic composite laminate consolidation", Ph.D. dissertation, Univ. of Twente, Twente.
6. Z. Püspöki, M. Storath, D. Sage, M. Unser, "Transforms and Operators for Directional Bioimage Analysis: A Survey", Advances in Anatomy, Embryology and Cell Biology, vol. 219, Springer International Publishing, ch. 3, 2016.

Proceedings of the Composites 2024 International Conference
Seville, Spain – March 06 – 08, 2024
DOI: : https://doi.org/10.26799/cp-composites-2024

A Strategy Using Optical Coherence Tomography for Full Cross-Sectional Quality Assessment of Glass-Fiber-Reinforced Unidirectional Thermoplastic Tapes

Michael Wenninger[1], Karin Kloiber[1], Christian Marschik[1], Gerald Berger-Weber[2]

[1]Competence Center CHASE GmbH, Hafenstraße 47-51, 4020 Linz, Austria,
michael.wenninger@chasecenter.at
[2]Institute of Polymer Processing and Digital Transformation, Altenbergerstraße 69, 4040 Linz, Austria

Abstract

Optical coherence tomography (OCT), originally developed for biomedical diagnosis, has been demonstrated to be a powerful non-destructive and non-invasive method of detecting common defects in glass-fiber-reinforced polymer composites. While other studies focused mainly on the use of OCT in the analysis of thermoset composites, we

showed that OCT can be used to detect typical defects (e.g., gaps, dry fiber regions) in thermoplastic UD tapes at high resolution in both offline and inline experiments.

Here we present a fast statistical algorithm for automatic and full cross-sectional evaluation of UD tapes based on B-scans. It assesses the distribution of dry fiber regions and delivers visualizations suitable for use in a real-time setting.

Our algorithm was developed using data from an industrial-scale setup, and we show that, within an industrially relevant production speed range of up to 15 m/min, we are now able to monitor 120 mm wide (and potentially wider) UD tapes inline at a transverse resolution of 22 µm, producing only 21 MB of data per measurement.

Keywords: Thermoplastic UD tapes, optical coherence tomography, digitalization, unidirectional, glass-fiber-reinforced thermoplastics, inline monitoring, quality assurance, non-destructive testing, defect detection

1. Introduction

A set of proposals has been adopted by the European Commission for the EU's climate, transport, energy, and taxation policies to reduce net greenhouse gas emissions to at least 45 % of their 1990 levels by 2030 [1]. Reducing vehicle weight (and thus saving fuel and increasing range) is an important step towards reaching these ambitious goals and can be achieved by using continuous fiber-reinforced thermoplastic composites. The methods for producing polymer composites with constant cross sections are based mostly on the pultrusion technique [2]. Continuous carbon or glass fibers, laid in parallel and flat, are pulled through an impregnation die, in which the fibers are penetrated by a thermoplastic polymer melt provided by an extruder. Unidirectional (UD) tapes (with fibers aligned in one load direction) are a special case of thin pultruded semi-finished films, the quality of which strongly affects final product quality (see Fig. 1 for a schematic of a typical UD tape production line). These UD tapes can be cut, stacked, consolidated and potentially also functionalized to create final products with local and weight-optimized reinforcement, for instance, for the aerospace or automotive industries. Common production defects (e.g., gaps and incompletely impregnated fibers) degrade visual appearance and mechanical performance. Detection of these defects during the production process enables timely corrective intervention to improve quality.

DOI: : https://doi.org/10.26799/cp-composites-2024

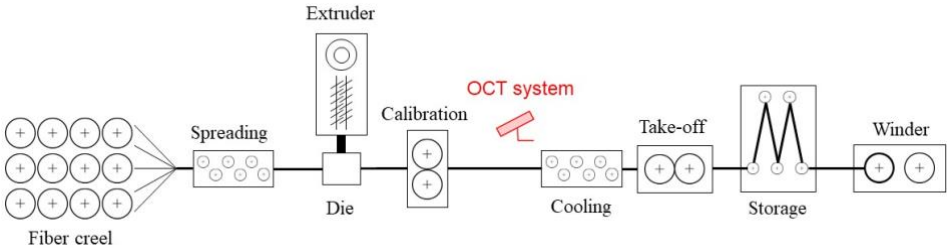

Fig. 1: Schematic of a typical UD tape production process including an integrated OCT system for quality assurance.

Optical coherence tomography (OCT) has been applied in several non-destructive testing (NDT) tasks, as it is non-invasive, fast, and offers high-resolution imaging of internal structures within semi-transparent media. Several studies have used OCT to investigate thermoset-based, glass-fiber-reinforced polymer composites (mainly epoxy resins) [3–6].

However, comparatively little attention has been directed towards its benefit in analyzing thermoplastic composites. Our previous studies [7–9] confirmed the ability of OCT to assess the quality of glass-fiber reinforced UD tapes in offline and inline measurements with both stationary and moving UD tapes. Optimal sensor settings were derived from a comprehensive experimental study performed on an industrial-scale UD-tape production line to achieve satisfactory measurement accuracy with acceptable data size [9].

In this work, we present a fast and robust algorithm for the full cross-sectional analysis of 120 mm wide UD tapes, with special focus on dry fiber regions with a critical width of at least 220 µm. Defects that are wider than the tape thickness are typically considered critical (according to industrial convention). Quality assessment (QA) methods in the tape production process are still based mainly on visual evaluation and rely on the operator's experience. Our approach to automation and objective evaluation forms the basis for more reliable QA. Further, it enables (and is a prerequisite for) virtual representation of the production line (Digital Twin) in the context of the fourth industrial revolution.

2. OCT: Technology and Equipment

OCT is an optical, non-destructive, and non-invasive imaging technique that operates in the near-infrared (NIR) spectral range. It was first introduced in ophthalmology in the 1990s [10] and has since been used in a growing range of applications both in biomedicine and material science [11, 12]. OCT exploits low-coherence interferometric phenomena to obtain structural information within turbid samples which strongly scatter light. Light sources, typically with high spatial but low temporal coherence, operating in the wave length range between 1-15 µm enable excellent axial resolution in the lower µm range [13]. OCT generates depth-resolved scans of signals reflected/back-scattered at internal or external structural sites or interfaces and is well suited to detecting features, in which the image contrast results from inhomogeneities of the refractive index within the sample [14]. For detailed information on the OCT measurement principle see [8, 9].

In our investigations, we used a commercial SD-OCT system (Thorlabs Telesto TEL321) that provides a maximum pixel density of 1024 per A-scan. It operates at a center wavelength of 1300 nm and is equipped with an OCT-LK4 lens kit from Thorlabs that has a working distance of 41.6 mm, a maximum field of view of 16x16 mm², and a numerical aperture of 0.042. The maximum possible imaging depth (strongly dependent on the sample medium) is 3.5/2.6 mm in air/water, which is sufficient to allow investigation of UD tape samples with typical thicknesses between 0.1 and 0.4 mm. The maximum A-scan sampling frequency is limited to 146 kHz with a sensitivity of 91 dB.

3. Experimental

3.1. Experimental setup

Experiments were performed on an industrial-scale UD-tape production line (Leistritz Extrusionstechnik GmbH, Nuernberg, Germany) located at the LIT Factory of Johannes Kepler University Linz (Linz, Austria). Its main components are shown schematically in Fig. 1. In this study, the line was used to pull through prefabricated UD tape samples, which is why the system setup from Fig. 1 was reduced considerably: Fiber creel, spreading unit and extruder were not used at all, and other components just for tape guidance or take-off.

DOI: : https://doi.org/10.26799/cp-composites-2024

Obviously, measuring prefabricated tape samples has the advantage of significantly reducing overall process complexity, as fiber spreading and impregnation are highly complex and critical process steps. Additionally, it allows tapes of different (but known) qualities to be investigated systematically. Fig. 2 (a) illustrates the final measurement setup, which included a base unit to which a 2D portal system and an OCT sensor head were attached. Fig. 2 (b) visualizes the measurement pattern for a moving sensor and tape. For more information about the setup and the step-by-step measurement procedure see [8].

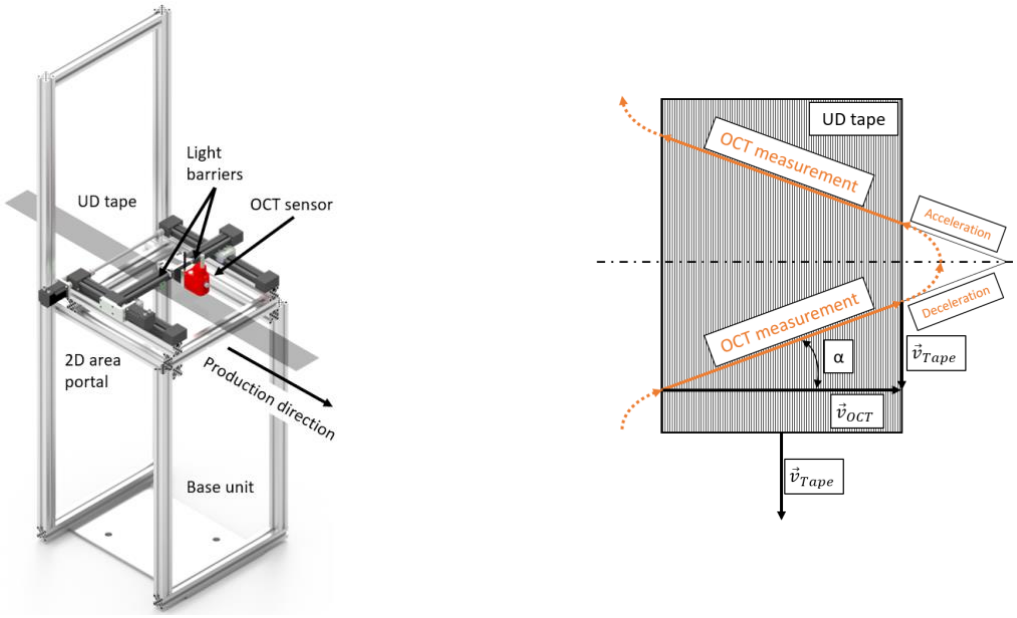

(a) (b)

Fig. 2: (a) Schematic of the measurement setup: a base unit with 2D portal system and OCT sensor head attached; (b) OCT measurement lines created for a moving UD tape.

3.2. UD-tape samples and test conditions

Prefabricated UD-tape samples that consisted of a thermoplastic polycarbonate (PC) matrix and glass fibers (GF) with a fiber volume content of approximately 44% were used for this investigation. The tape was 0.2 mm thick and 120 mm wide. The GF had a filament diameter of 17 µm, a linear density of 2400 tex (g/km), a solid density of 2620 kg/m³, and a tensile strength between 2200 and 2500 MPa. The PC had a glass transition temperature of 145 °C, a melt flow rate of 37 g/10min (300 °C/1.2 kg), and a solid density of 1192 kg/m³.

Using the inline settings derived in [9] (A-scan sampling rate: 146 kHz, OCT travel speed: 0.4 m/s, A-scan averaging: 8) yielded a transverse resolution of 22 µm between two adjacent A-scans. The measurements were conducted at a UD-tape take-off speed of 10 m/min.

4. Evaluation algorithm

With the aim of efficient real-time monitoring, we defined a workflow for the detection of dry fiber regions across the entire tape cross section; it is based on grayscale analysis of the OCT raw data (B-scan), where bright sections indicate centers of strong dispersion, which correspond to dry fiber domains (see [8]). The algorithm comprises the following steps: The OCT raw data is cropped along the tape edges (as the high intensity there would interfere with the algorithm). The greyscale values within buckets of 10 adjacent A-scans are averaged, where the total width per bucket is 220 µm, which corresponds to the minimum relevant defect. Subsequently, the OCT data is binarized by using the global median of the grayscale image as threshold. Using the binarized data array, a trace along the center of the tape cross section can be created to detect dry fiber regions (each of which is an event with a value of 1). Based on this trace, the distribution of widths of dry regions along the entire cross section can be assessed, which – together with the overall dry-fiber content – allows tape quality to be evaluated.

5. Results and Discussion

Fig. 3 (a) and (b) present the results for a poor-quality tape sample with an apparent dry-fiber content of roughly 34%. The widest dry fiber region is approximately 2 mm wide, and the mean dry region is about 1 mm. In

DOI: : https://doi.org/10.26799/cp-composites-2024

comparison, (c) and (d) show the results for a tape section of much higher quality, with a dry content of around only 2%. Here, the histogram indicates fewer and shorter dry regions (maximum width of 0.44 mm and a mean of 0.33 mm), and a clear separation between dry and impregnated tape regions.
Note that different tape take-off speeds have only a minor influence on the transverse resolution, but a significant impact on information loss (i.e., on the minimum defect length that can be captured) between two consecutive measurements of the OCT sensor moving in alternating directions across the tape surface.

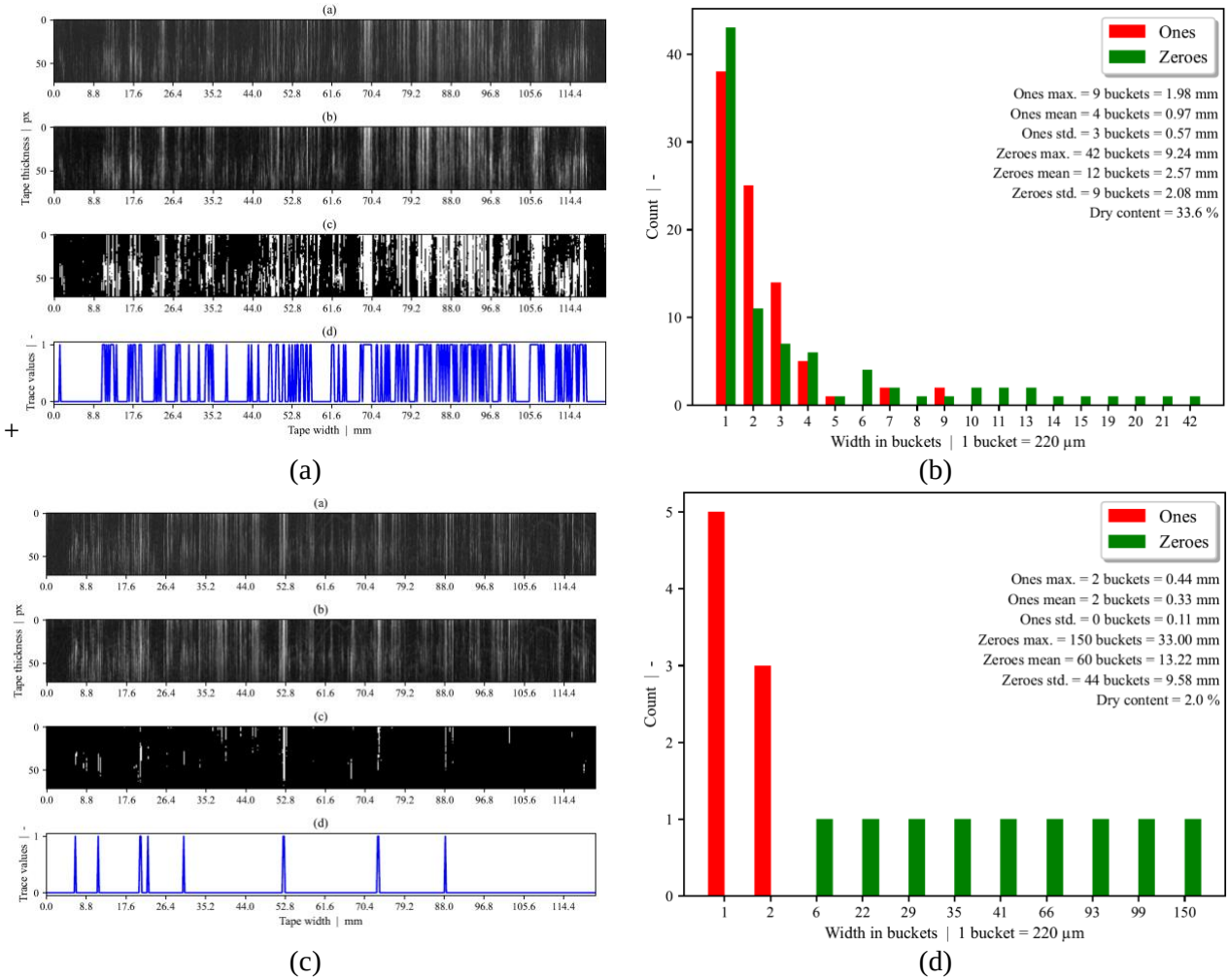

Fig. 3: Comparison between a poor-quality tape region ((a) and (b)) with a dry content of around 34% and a higher-quality one ((c) and (d)) with a dry content of only 2%, both measured at a take-off speed of 10 m/min.

6. Conclusion and Outlook

We extended our previous research into OCT as a novel inline monitoring technique for the thermoplastic UD-tape production process by developing a fast and robust evaluation algorithm for the full cross-sectional analysis of 120 mm wide tapes that provides statistical information about the dry-region distribution (in particular, the maximum defect width, the mean defect width, and the overall extent of defects relative to tape width). Although some steps of the workflow are not yet fully automated - OCT raw data preprocessing in particular is complicated by fluctuations in tape guidance - we see tremendous potential in using OCT in a real-time setting, as both data recording and evaluation are fast, moreover, subjective judgement based on visual inspection is eliminated.

Future research could improve tape guidance (and thus enable full automation of the procedure) or optimize for a faster OCT travel speed to allow shorter defects in the fiber direction to be detected.

DOI: : https://doi.org/10.26799/cp-composites-2024

Acknowledgements

The authors acknowledge financial support through the COMET Centre CHASE, funded within the COMET − Competence Centers for Excellent Technologies program by the BMK, the BMDW and the Federal Provinces of Upper Austria and Vienna. The COMET program is managed by the Austrian Research Promotion Agency (FFG).

References

[1] European Commission, A European Green Deal - Striving to be the first climate-neutral continent. [Online]. Available: https://commission.europa.eu/strategy-and-policy/priorities-2019-2024/european-green-deal_en (accessed: 2023).

[2] K. Minchenkov, A. Vedernikov, A. Safonov, and I. Akhatov, "Thermoplastic Pultrusion: A Review," *Polymers*, vol. 13, no. 2, 2021, doi: 10.3390/polym13020180.

[3] J. P. Dunkers *et al.*, "Optical coherence tomography of glass reinforced polymer composites," *Composites Part A: applied science and manufacturing*, vol. 30, pp. 139–145, 1998.

[4] K. Wiesauer, M. Pircher, E. Götzinger, C. K. Hitzenberger, R. Oster, and D. Stifter, "Investigation of glass–fibre reinforced polymers by polarisation-sensitive, ultra-high resolution optical coherence tomography: Internal structures, defects and stress," *Composites Science and Technology*, vol. 67, 15-16, pp. 3051–3058, 2007, doi: 10.1016/j.compscitech.2007.04.018.

[5] J. P. Dunkers, D. P. Sanders, D. L. Hunston, M. J. Everett, and W. H. Green, "Comparison of optical coherence tomography, x-ray computed tomography, and confocal microscopy results from an impact damaged epoxy/e-glass composite," *The Journal of Adhesion*, vol. 78, no. 2, pp. 129–154, 2002.

[6] D. Stifter *et al.*, "Investigation of polymer and polymer/fibre composite materials with optical coherence tomography," *Meas. Sci. Technol.*, vol. 19, no. 7, 2008, doi: 10.1088/0957-0233/19/7/074011.

[7] M. Wenninger, C. Marschik, K. Felbermayer, B. Heise, G. Berger-Weber, and G. Steinbichler, "Optical Coherence Tomography - A New Method for Evaluating The Quality of Thermoplastic Glass-Fiber-Reinforced Unidirectional Tapes," in *Conference Proceedings of the 37th International Conference of the Polymer Processing Society*: AIP Publishing, 2022.

[8] M. Wenninger, C. Marschik, K. Felbermayer, B. Heise, T. Kranzl, and G. Steinbichler, "A novel measurement approach based on optical coherence tomography for inline quality assessment of thermoplastic glass-fiber reinforced unidirectional tapes," *Journal of Thermoplastic Composite Materials*, 089270572211433, 2022, doi: 10.1177/08927057221143371.

[9] M. Wenninger, C. Marschik, M. Schnaitter, G. Hochleitner, G. Berger-Weber, and G. Steinbichler, "Using Optical Coherence Tomography to Evaluate the Optimal Settings for Inline Detection of Defects in Glass-Fiber-Reinforced Unidirectional Thermoplastic Tapes," in *Conference Proceedings of the 38th International Conference of the Polymer Processing Society*: AIP Publishing, 2023.

[10] V. Srivastava, T. Anna, M. Sudan, and D. S. Mehta, "Tomographic and volumetric reconstruction of composite materials using full-field swept-source optical coherence tomography," *Meas. Sci. Technol.*, vol. 23, no. 5, p. 55203, 2012, doi: 10.1088/0957-0233/23/5/055203.

[11] A. F. Fercher, C. K. Hitzenberger, W. Drexler, G. Kamp, and H. Sattmann, "In Vivo Optical Coherence Tomography," *American Journal of Ophthalmology*, vol. 116, no. 1, pp. 113–114, 1993, doi: 10.1016/S0002-9394(14)71762-3.

[12] D. Stifter, "Beyond biomedicine: a review of alternative applications and developments for optical coherence tomography," *Appl. Phys. B*, vol. 88, no. 3, pp. 337–357, 2007, doi: 10.1007/s00340-007-2743-2.

[13] W. Drexler *et al.*, "In vivo ultrahigh-resolution optical coherence tomography," *Optics Letters*, vol. 24, no. 17, 1999.

[14] A. Nemeth, G. Hannesschlager, E. Leiss, K. Wiesauer, and M. Leitner, "Optical Coherence Tomography – Applications in Non- Destructive Testing and Evaluation," in *Optical Coherence Tomography*, M. Kawasaki, Ed.: InTech, 2013.

Proceedings of the Composites 2024 International Conference
Seville, Spain – March 06 – 08, 2024
DOI: : https://doi.org/10.26799/cp-composites-2024

An experimental investigation of the spreading behaviour of carbon-fiber rovings

S. Kohl [1,*], C. Marschik [1], T. Kranzl [2], M. Schnaitter [2], G. R. Berger-Weber [2]

[1] Competence Center CHASE GmbH
Hafenstraße 47-51, 4020 Linz, Austria, stefan.kohl@chasecenter.at
[2] Institute of Polymer Processing and Digital Transformation
Johannes Kepler University Linz, Linz, Austria

Abstract

This work investigated the production of UD tapes based on a continuous extrusion process: Multiple fiber rovings are unwound from a creel and spread mechanically to a certain width to form a homogeneous fiber carpet. The fiber carpet is then impregnated with thermoplastic polymer melt while being pulled through an extrusion die. Impregnation between the fibers must be complete to ensure good fiber-matrix adhesion in the tape, which is essential for transferring mechanical loads in the final application. In the downstream processing steps, the tape is calibrated to the final thickness, cooled, and rolled up.

An integral step of the process is fiber spreading. A perfectly spread and homogeneous fiber carpet is a prerequisite for complete fiber impregnation and thus a sufficiently high tape quality. Various techniques may be used to spread rovings from their initial to the required width. From these, we systematically studied the factors that affect deflection-based fiber spreading, which is a technique that applies higher stress to the outer roving filaments, they evade to smaller radii, which widens the roving.

A test rig was developed to investigate fiber spreading under near-process conditions. Using a carbon fiber roving, numerous spreading tests were carried out in which the roving was guided over deflection rods and the evolving roving width was recorded with cameras before and after spreading. In these experiments, (i) the number of rods, (ii) the rod diameter, (iii) the rod immersion depth, and (iv) the roving take-off speed were varied. It could be shown that the spreading behavior is mainly affected by the number of rods and to a lesser extent by the immersion depth.

The results of the test-rig experiments shall be used to optimize the spreading configuration in the industrial production of UD tapes later on.

Keywords: UD tapes, carbon fibers, fiber spreading, spreading by deflection

1. Introduction

To achieve the European Union's climate target of climate neutrality by 2050, efficient solutions are needed in the transportation sector, especially in the aircraft and automotive industries [1]. Employing components with continuous fiber-reinforced plastics decreases pollution by reducing component weight and thus fuel consumption while providing the same mechanical performance as their metallic counterparts [2–5]. Due to their excellent mechanical properties, unidirectional (UD) fiber-reinforced thermoplastic tapes are used increasingly for targeted local reinforcement of structural components in applications that require light-weight [6].

An essential prerequisite in the production of high-quality UD tapes is a homogeneously spread roving with a constant spread width. In 1996, Wilson [7] studied the lateral expansion of polyamide fiber rovings and cotton yarns, and developed a model for estimating the spread width when using a spreader rod. Irfan [8] extended this model to include the behavior of glass-fiber rovings and to estimate the spread width on a second spreader rod. Both models were validated by idealized experiments of limited industrial relevance. Wilson performed purely static experiments in which a roving was placed under tension. Irfan, in contrast, investigated spreading by cyclically pulling the roving under tension over spreader rods and then releasing the tension. In both studies, tension was achieved by attaching a weight.

In this work, we systematically investigated fiber spreading by deflection, using a new, process-oriented test rig. Experiments were carried out to examine the effects of (i) the number of rods, (ii) the rod diameter, (iii) the rod immersion depth, and (iv) the take-off speed on the spreading behavior of a 24K carbon-fiber roving. For

Proceedings of the Composites 2024 International Conference
Seville, Spain – March 06 – 08, 2024
DOI: : https://doi.org/10.26799/cp-composites-2024

each test configuration, the roving was recorded by cameras before and after spreading, and the widths were calculated via image processing. Validation of the above-mentioned models is not discussed in this work.

2. Experimental

A test rig with integrated optical width measurement was developed to investigate fiber spreading by deflection. A roving was continuously pulled through the test stand, and initial and final spreading widths were recorded. For systematic analysis, various spreading setups were realized by adjusting number and diameter of the rods, immersion depth, and take-off speed of the roving.

2.1 Material

A carbon fiber roving, Tenax-E STS40 E23 24K 1600 tex from Teijin, was used. The fiber bundle consisted of 24000 filaments with an average filament diameter of 7 µm and an epoxy resin sizing.

2.2 Test setup

In order to investigate the main influencing parameters in fiber spreading by deflection, a test rig, the main components of which are shown schematically in Fig. 1(a), was developed. A single roving was unwound from a fiber spool by a winder at a controlled take-off speed and pulled through the spreading setup, which consisted of a variable number of metallic spreader rods of a predefined diameter whose horizontal and vertical distances to each other could be adjusted individually. The initial and final spreading widths of the roving were determined by means of two line-scan cameras mounted before and after spreading, respectively. Two monochrome line-scan cameras of the type NECTA N4K-3 from Alkeria with a sensor (AMS DR4K3.5) with 1x4096 pixels and a pixel size of 3.5 µm were used. A Ricoh FL-BC7528 lens with a minimum working distance of 250 mm and a focal length of 75 mm was employed. The recording frequency of the line scan cameras was adjusted to the roving take-off speed using a Baumer rotary encoder mounted on a 30 mm diameter roller. The number of encoder ticks was defined based on the pixel width in the transverse direction to ensure that there was no distortion and that $\Delta x = \Delta y$ applied to each pixel. Here, Δx and Δy correspond to the length information of a pixel in the longitudinal and transverse directions, respectively. Fiber tension before and after spreading was recorded by means of load cells.

To ensure that both cameras captured the same area of the roving, they were synchronized using a Python script. The recording scheme is shown in Fig. 1(b). Recording was started with the infeed camera, the encoders of both cameras were set to zero (1), and the infeed width was recorded over a defined roving length (2)-(3). Meanwhile, the encoder ticks were counted and compared to the current roving length between the cameras. When the encoder ticks corresponded to the current length of the roving, the second camera started recording (4) until the same roving length had been recorded (5).

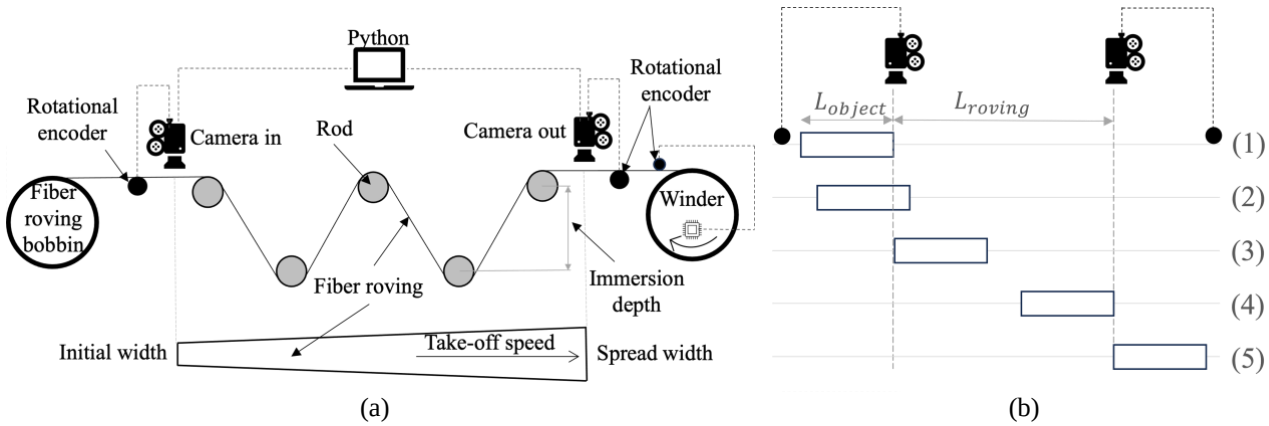

(a) (b)

Fig. 1: Schematic representations of (a) the test setup and (b) the synchronized image acquisition process.

2.3 Procedure

Two experimental designs were employed to systematically investigate the influences of rod radius and number of rods at various immersion depths and take-off speeds. The spreader rods were arranged symmetrically in a zigzag pattern such that the roving passed over one rod and under the next. The test parameters used for the 190 different test configurations are listed in **Error! Reference source not found.**.

DOI: : https://doi.org/10.26799/cp-composites-2024

Table 1: Parameters iterated in the experiments

	Unit	Investigating the role of rod diameter	Investigating the role of number of rods
Rod diameter	mm	15, 30, 45	15
Number of rods	-	5	3, 5, 7, 9
Rod distance	mm	58	
Immersion depth	mm	40, 50, 60, 70	20, 30, 40, 50, 60, 70
Take-off speed	m/min	1, 2, 3, 4, 5	

In our experiments, five images were recorded for each spreading setup over a roving length of 94.25 mm (one encoder revolution) immediately before the first and directly after the last spreader rod. The roving width was computed in Python using image binarization in combination with an edge detection algorithm. The number of pixels was then used to determine the roving width over the predefined length. For further processing, a mean width was calculated from each image, the mean widths of the five images for each setup were averaged, and then the spread ratio (Eqs. (1)) and its standard deviation (Eqs. (1) – (2)) were calculated using error propagation.

$$w_{ratio} = \bar{w}_{final}/\bar{w}_{initial}, \tag{1}$$

$$s_i = [(\sum_{i=1}^{n}(w_i - \bar{w})^2) \cdot (n-1)^{-1}]^{0.5} \text{ and} \tag{2}$$

$$s_{i,ratio} = w_{i,ratio} \cdot \left[\left(s_{i,initial}/\bar{w}_{i,initial}\right)^2 + \left(s_{i,final}/\bar{w}_{i,final}\right)^2\right]^{0.5} \cdot N^{-0.5}, \tag{3}$$

where w_{ratio}, w and s are the spread ratio, the roving width and the standard deviation, respectively.

3. Results

Fig. 2(a) shows the relationship between spread ratio and take-off speed for various numbers of spreader rods. For a constant number of rods, the take-off speed had minor impact on the spread ratio. Similarly, the spreading performance remained roughly the same with increasing pull-off speed. We attribute minor variations to the variable input width of the roving unwound from its spool. In contrast, the more rods were used, the more extensively the roving was spread. The mean spread ratio for three rods was 1.16, which almost doubled to 2.16 when nine rods were employed. No significant influences of immersion depth or rod diameter on the spread ratio were observed when the number of rods was kept constant (see Fig. 2(b)). The average spread ratios for the 15 mm, 30 mm, and 45 mm diameters were 1.49, 1.51, and 1.48, respectively. Considering the standard deviation in each case, rod diameter seems to have had no impact on spreading.

As can be seen in Fig. 3(a), with increasing number of rods, spreading performance improved. Further, the influence of the immersion depth grew with rising number of rods. For example, as the immersion depth increased from 20 mm to 50 mm, the increase in spread ratio was 0.03 for five rods, 0.43 for seven rods, and 0.58 for nine rods. For three rods, we observed no effect of immersion depth. The curves for seven and nine rods could not be plotted over the full range of x-values because at greater immersion depths these high numbers of rods resulted in forces acting on the roving that exceeded 300 N – the load limit of the test rig. For instance for three rods, the force increased only from 11 N to 27 N when the immersion depth was increased from 20 mm to 50 mm. In contrast, using nine rods increased 66 N to 228 N, as shown in Fig. 3(b), in other words a strong positive interaction of immersion depth and number of rods was found Thus changing from three to nine rods increased the force by approximately a factor of 10. In our case, we reached the maximum load limit of the test rig with nine rods.

DOI: : https://doi.org/10.26799/cp-composites-2024

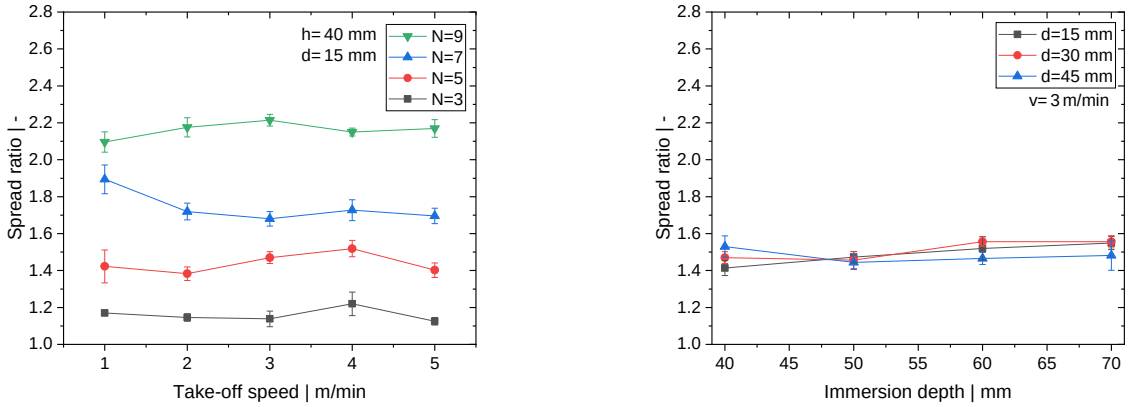

(a) (b)

Fig. 2: Spread ratio as a function of (a) the take-off speed for various numbers of spreader rods and (b) the immersion depth for five rods of various diameters.

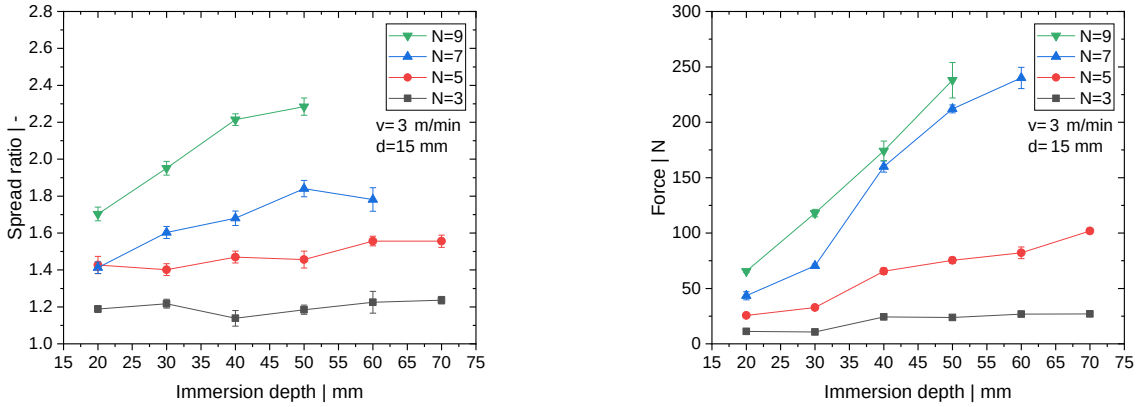

(a) (b)

Fig. 3: (a) Spread ratio and (b) forces acting on the fiber roving as functions of immersion depth for various numbers of spreader rods.

4. Conclusion

In this study, we examined the effects of the number of rods, rod diameter, rod immersion depth, and take-off speed, on fiber spreading. To this end, a test rig that optically measured initial and final roving widths was developed. The results showed that the spread width is largely unaffected by variations in take-off speed and rod diameter. In contrast, the spreading performance improved substantially with increasing number of spreader rods. For example, by increasing the number of rods from three to nine at an immersion depth of 50 mm, we were able to achieve a spread ratio of 2.28, thus more than doubling the initial width. The improved spreading performance, however, goes hand in hand with an increase in roving tension. For a more detailed analysis, additional statistical investigations will be conducted as part of future research. In addition, different types of fiber roving, the influence of rod surface roughness, and the influence of temperature should be investigated.

Acknowledgements

The authors acknowledge financial support through the COMET Centre CHASE, funded within the COMET − Competence Centers for Excellent Technologies programme by the BMK, the BMDW and the Federal Provinces of Upper Austria and Vienna. The COMET programme is managed by the Austrian Research Promotion Agency (FFG).

DOI: : https://doi.org/10.26799/cp-composites-2024

References

[1] European Commission, "Communication from the Commission to the EuropeanParliament, the European Council, the Council, the European Economic and SocialCommittee and the Committee of the Regions-The European Green Deal," 2019.

[2] Tapajyoti Ghosh, Hyung Chul Kim, Robert De Kleine, Timothy J. Wallington, and Bhavik R. Bakshi, "Life cycle energy and greenhouse gas emissions implications of using carbon fiber reinforced polymers in automotive components: Front subframe case study," *Sustainable Materials and Technologies*, vol. 28, e00263, 2021, doi: 10.1016/j.susmat.2021.e00263.

[3] Eri Amasawa, Mikiaki Hasegawa, Naoki Yokokawa, Hirokazu Sugiyama, and Masahiko Hirao, "Environmental performance of an electric vehicle composed of 47% polymers and polymer composites," *Sustainable Materials and Technologies*, vol. 25, e00189, 2020, doi: 10.1016/j.susmat.2020.e00189.

[4] Sujit Das, Diane Graziano, Venkata K.K. Upadhyayula, Eric Masanet, Matthew Riddle, and Joe Cresko, "Vehicle lightweighting energy use impacts in U.S. light-duty vehicle fleet," *Sustainable Materials and Technologies*, vol. 8, pp. 5–13, 2016, doi: 10.1016/j.susmat.2016.04.001.

[5] U. K. Vaidya and K. K. Chawla, "Processing of fibre reinforced thermoplastic composites," *International Materials Reviews*, vol. 53, no. 4, pp. 185–218, 2008, doi: 10.1179/174328008X325223.

[6] K. Michael, M. Mathias, N. Thomas, and A. Volker, "From UD-tape to Final Part – A Comprehensive Approach Towards Thermoplastic Composites," *Procedia CIRP*, vol. 66, pp. 96–100, 2017, doi: 10.1016/j.procir.2017.03.371.

[7] S. D. R. Wilson, "Lateral spreading of fibre tows," *Journal of Engineering Mathematics*, vol. 32, no. 1, pp. 19–26, 1997, doi: 10.1023/A:1004253531061.

[8] M. S. Irfan *et al.*, "Lateral spreading of a fiber bundle via mechanical means," *Journal of Composite Materials - J COMPOS MATER*, vol. 46, pp. 311–330, 2012, doi: 10.1177/0021998311424624.

Proceedings of the Composites 2024 International Conference
Seville, Spain – March 06 – 08, 2024
DOI: : https://doi.org/10.26799/cp-composites-2024

Numerical Simulation of Thermal Frontal Polymerization in Polymer Composites: The Role of Nanoparticle Fillers

Margit Lang[1], Christoph Schmidleitner[1,2], Peter Fuchs[1], Elisabeth Rossegger[1]

[1]Polymer Competence Center Leoben GmbH (PCCL), Sauraugasse 1, 8700 Leoben, Austria, margit.lang@pccl.at
[2]Institute for Chemistry and Technology of Materials, University of Technology of Graz, NAWI Graz Stremayrgasse 9, 8010 Graz, Austria, christoph.schmidleitner@pccl.at

Abstract

Given the global priority of sustainability and waste reduction, polymer composites play an important role in enabling high-performance, lightweight structures and increasing product lifespans by decades due to corrosion resistance and durability. At the same time, innovative curing and polymerization processes must exhibit improved efficiencies and reduced environmental impact. In this context, frontal polymerization (FP) has emerged as a low-energy alternative that enables rapid and energy efficient manufacturing of composites compared to conventional processes, thus providing a promising strategy to adress sustainability challenges. However, sustaining FP in composites using highly conductive fillers is challenging due to the increased energy dissipation and reduced availability of exothermic energy as the filler content increases at the cost of resin volume fraction. The detailed compilation of fundamental material data and their subsequent usage in Modelling & Simulation routines, like presented in this work for Fe_3O_4 (iron-oxide, magnetite) nanoparticle fillers added to a Bisphenol A Diglycidyl Ether (BADGE) resin system, provides insight into the thermo-chemical process and the inhibitory effects of the nanoparticles, i.e. influence on the key characteristics of FP like maximum temperature, front shape, and front velocity.

Keywords: Thermal Frontal Polymerization (TFP), Polymer Composites, Nanoparticle Fillers, Polymerization, Front, Heat Loss

1. Introduction

Frontal Polymerization (FP) is a technique that harnesses the chemical energy stored within a resin to drive material synthesis, thereby reducing the energy required for manufacturing compared to conventional methods [1]. In this self-sustained process, an initial stimulus (e.g., thermal or photo) induces a localized reaction zone, the so-called “polymerization front”, which can propagate through the entire system without requiring further energy input. Motivated by the substantial energy and time savings, offered by the FP approach compared to conventional manufacturing techniques, more advances have been made in the development and usage of this technique for the rapid fabrication of reinforced, highly filled polymer composites [2]. Furthermore, according to Li et al. [3] the extremely fast curing process of frontal polymerization is ideal for encapsulation of nanoparticles to inhibit sedimentation of particles. Given the fact that in TFP the frontal behavior is determined via the synergistic effect of heat generation from the exothermic reaction of the resin, the heat dissipation, and the thermal conductivity of the FP system, it is essential to study the influence of fillers on the curing behavior. The detailed compilation of fundamental material data and their subsequent usage in Modelling & Simulation routines is expected to enable the prediction of successful FP performance. Thus, in this study, a numerical approach for the detailed understanding of the inhibitory effects of different wt.% of Fe_3O_4 nanoparticles on the frontal polymerization of Bisphenol A Diglycidyl Ether (BADGE) is presented.

2. Materials

Bisphenol A Diglycidyl Ether (BADGE) (Product name: D.E.R. 332) as well as Fe_3O_4 (iron oxide, magnetite) nanoparticles with a size distribution of 50-100 nm and 1,1,2,2-Tetraphenyl-1,2-ethanediol (TPED) were purchased from Sigma Aldrich. The photo acid generator (4-n-octyloxyphenyl)-phenyliodonium hexafluoroantimonate (IOC8-SbF_6) was acquired from BLDpharm.

3. Material Characterization and Material Modeling

In FP the reaction process is mainly governed by the chemical and physical properties of the reacting system. Common criteria of FP like front initiation time, frontal velocity, and frontal temperature are strictly dependent

DOI: : https://doi.org/10.26799/cp-composites-2024

on the intrinsic properties of the materials used in the reaction system, such as the reactivity of the resin formulation and the thermal properties. Thus, a detailed material characterization and modeling including the enthalpy of the cure reaction, reaction kinetics, temperature dependent specific heat, temperature dependent thermal conductivity, and density was performed for the unfilled BADGE resin as well as BADGE with different filling degrees (10, 20, 30 wt.%) of Fe_3O_4 nanoparticles. Since the scope of this study is to predict the frontal behavior of further resin compositions (i.e., different wt.% of fillers) the respective material parameters, needed as input for the simulations, were extrapolated, e.g. using regression techniques and the rule of mixtures (RoM). Furthermore, since the reactive medium is embedded in a silicone cylinder (as described in detail in Section 5.1) the required Silicone material parameters (thermal conductivity, specific heat, density) were also determined experimentally.

4. Computational Modelling

4.1. Model Setup

The computational domain, used in this study, is shown schematically in Figure 1. A channel, filled with the reactive medium BADGE with a radius R_C = 5mm and length L=25mm is embedded in a hollow Silicone cylinder with an outer radius of $R_{Silicone}$ = 7mm. Adiabatic boundary conditions are assumed. In the initial stage, the whole domain is at a uniform temperature of T_0 = 25°C. The ignited boundary is subjected to a fixed temperature $T_{trigger}$ = 300°C for an initiation time of $t_{trigger}$ = 20s. After initiation of the front, the triggering source is removed for the remainder of the simulation, see Figure 1(b).

4.2. Thermo-Chemical Modelling

Successful FP requires a delicate balance of reaction rates, exothermicity, and efficient heat transport into unpolymerized media while minimizing the heat losses to the surroundings [4]. The total heat flow within the computational domain (see Section 5.1.) can be described by the axisymmetric heat transfer equation expressed as

$$\rho c_p \frac{\partial \mathrm{T}}{\partial t} = \rho H_r \frac{\partial \alpha}{\partial t} + \kappa \left(\frac{\partial^2 T}{\partial r^2} + \frac{1}{r}\frac{\partial T}{\partial r} + \frac{\partial^2 T}{\partial z^2} \right) \quad (1)$$

where ρ is the density (in kg/m³), c_p is the specific heat (in J/kgK), H_r is the total heat of reaction (in kJ/kg), and κ is the thermal conductivity (in W/mK).
An important step towards the simulation of the entire process of FP is the selection of a suitable mathematical model to describe the reaction kinetics (thermokinetics) of the resin system to relate the time and temperature evolution in the reaction channel to the heat produced by the reaction itself. The model adopted in this numerical study characterizes the reaction rate simply as a function of time, temperature and conversion:

$$\frac{\partial \alpha}{\partial t} = k(T) \cdot f(\alpha) = A exp\left(\frac{-E_\alpha}{RT}\right) \cdot (1-\alpha)^n \alpha^m \quad (2)$$

where $k(T)$ normally takes the form of the Arrhenius equation [5] and $f(\alpha)$ represents the reaction type describing the dependency of the reaction rate on conversion. In the above equation A is the pre-exponential factor (in 1/s), E_α is the activation energy (in J/mol), R is the universal gas constant which has the value of 8.314 J/molK, and T is an absolute temperature (in K). In the current study, the autocatalytic Prout-Tompkins model is considered as most appropriate where $(1-\alpha)$ corresponds to the relative amount of reactant, α corresponds to the relative amount of product, and m and n represent the reaction order (i.e., kinetic exponents). The constants of the curing kinetics model, see Equation (1) are obtained by solving a nonlinear optimization problem based on the multiple regression technique. The optimization solver minimizes the error between the $d\alpha/dt - T$ curves extracted from Differential Scanning Calorimetry (DSC) test data and the curves obtained by the chosen cure kinetic model.

DOI: : https://doi.org/10.26799/cp-composites-2024

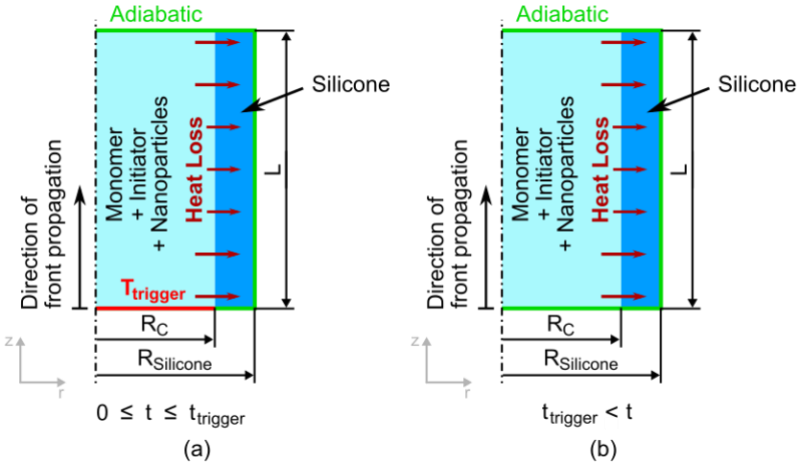

Figure 1: Model setup: geometrical model and boundary conditions.

4.3. Numerical Implementation

The frontal polymerization characteristics of the BADGE resin with different wt.-% of Fe_3O_4 nanoparticles is predicted using an ABAQUS heat transfer analysis with the subroutines HETVAL and USFLD, see Figure 2. The heat which is generated from the exothermic reaction cannot be directly defined in the ABAQUS input file. Thus, a so-called Heat Flux Subroutine (HETVAL) must be used to update the volumetric heat flux at each time increment for solving the current heat transfer problem. The User Defined Field Subroutine (USDLFD) updates the degree of cure as well as the rate of cure at each integration point and each time increment based on the cure kinetics model which serves as input for the HETVAL subroutine.

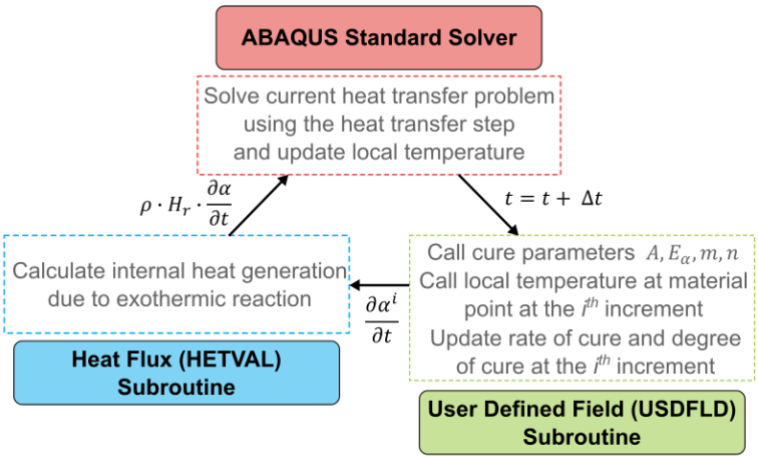

Figure 2: Numerical implementation of TFP in ABAQUS with subroutines USDFLD and HETVAL.

5. Results and Discussion

In this section the results of the numerical simulation and the influence of different wt.% of Fe_3O_4 nanoparticles on the key characteristics of frontal polymerization are shown.

In thermal frontal polymerization the interplay between heat diffusion and Arrhenius type reaction kinetics gives rise to the propagating reactive front which is effectively sustained through a system positive feedback mechanism.

Figure 3(a) shows the contour plots for different filling degrees where the heat flux for the unfilled BADGE is clearly more concentrated compared to higher filling degrees. Furthermore, it gets clear that the system with the highest filling degree of nanoparticles doesn't create enough heat to sustain a self-propagating polymerization front. This correlates well with experiments which showed a critical filling degree of 30 wt.% above which front propagation couldn't be observed. Due to the boundary conditions (i.e., heat loss to the

DOI: : https://doi.org/10.26799/cp-composites-2024

surrounding Silicone) the front shape is convex. Figure 3(b) shows the influence of different filling degrees on the heat flux, i.e. by normalizing the respective results to the heat flux achieved with the unfilled system.

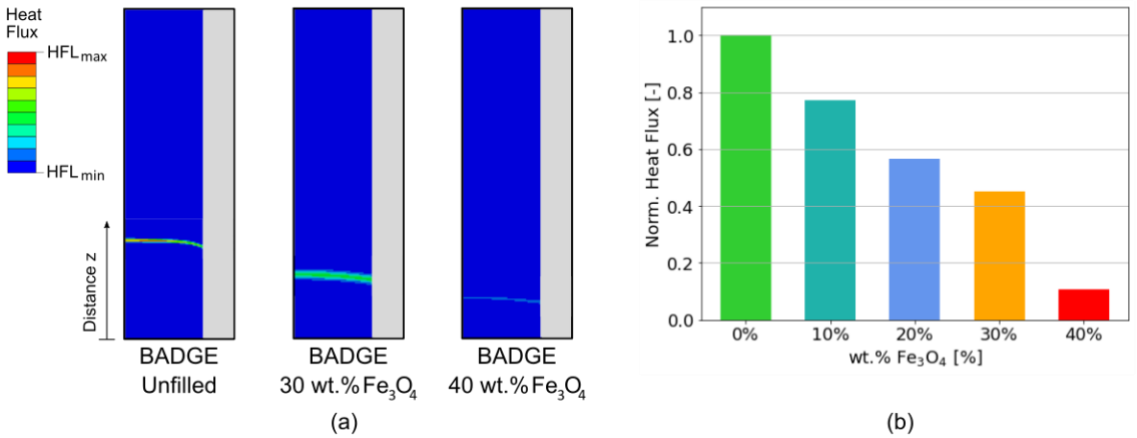

Figure 3: Heat generated by the exothermic reaction for different wt.% of Fe_3O_4 nanoparticles.

Figure 4 shows the relationship between the wt.% of nanoparticles and the key characteristics of FP, namely the frontal velocity and the frontal temperature. It is worth mentioning, that the front position versus time data for all systems (except the 40 wt.%) were found to be linear which indicates that self-sustaining fronts were achieved. An increasing filling degree leads to a decrease in frontal velocity and frontal temperature, attributed to the reduction in resin content resulting in a decrease in the released heat as well as higher heat diffusion.

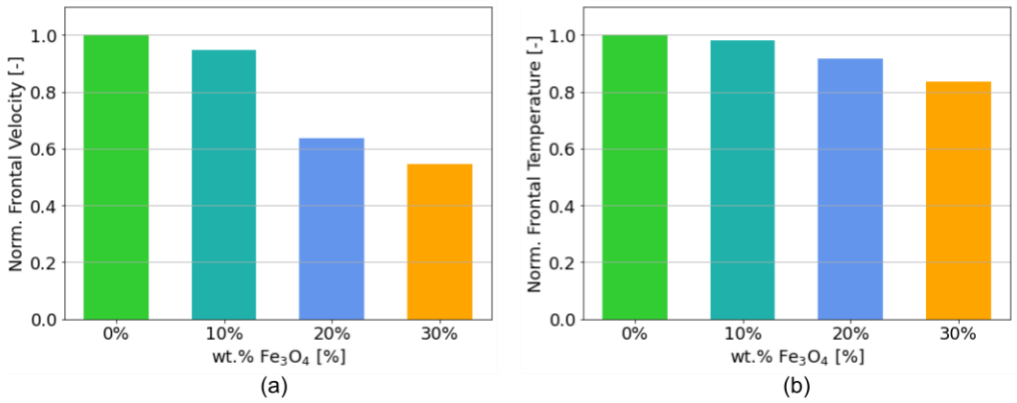

Figure 4: Influence of different wt.% of Fe_3O_4 nanoparticles on frontal velocity and frontal temperature.

6. Conclusion

In this study a comprehensive approach to study the influence of different filling degrees of nanoparticles with enhanced thermal conductivity based on numerical simulations was presented. Since in FP the reaction process is mainly governed by the chemical and physical properties of the reacting system an extensive material characterization of BADGE with different wt.% of Fe_3O_4 nanoparticles was conducted. In the modeling of dynamic frontal polymerization, a transient heat transfer equation with an internal heat generation term associated with the resin's exothermic reaction was solved to determine the polymerization characteristics. The results showed a critical filling degree of 30 wt.% above which front propagation couldn't be observed. Furthermore, a decrease in frontal velocity and frontal temperature with increasing filling degree was shown.

Acknowledgements

The research work was performed within the COMET-project 'Photostructurable Encapsulation Molds and Magnetic Composites' (project-no.: VII-S2) at the Polymer Competence Center Leoben GmbH (PCCL, Austria) within the framework of the COMET-program of the Federal Ministry for Climate Action, Environment, Energy, Mobility, Innovation and Technology and the Federal Ministry for Digital and Economic

Affairs with contributions by the Graz University of Technology. The PCCL is funded by the Austrian Governments and the State Governments of Styria, Lower Austria and Upper Austria.

References

1. Centellas, P. J.; Yourdkhani, M.; Vyas, S.; Koohbor, B.; Geubelle, P. H.; Sottos, N. R. (2022): Rapid multiple-front polymerization of fiber-reinforced polymer composites. In: *Composites Part A: Applied Science and Manufacturing* 158, S. 106931. DOI: 10.1016/j.compositesa.2022.106931.
2. Kumar, Aditya; Gao, Yuan; Geubelle, Philippe H. (2021): Analytical estimates of front velocity in the frontal polymerization of thermoset polymers and composites. In: *Journal of Polymer Science* 59 (11), S. 1109–1118. DOI: 10.1002/pol.20210155.
3. Li, Qing; Shen, Hai-Xia; Liu, Chang; Wang, Cai-Feng; Zhu, Liangliang; Chen, Su (2022): Advances in frontal polymerization strategy: From fundamentals to applications. In: *Progress in Polymer Science* 127, S. 101514. DOI: 10.1016/j.progpolymsci.2022.101514.
4. Suslick, Benjamin A.; Hemmer, Julie; Groce, Brecklyn R.; Stawiasz, Katherine J.; Geubelle, Philippe H.; Malucelli, Giulio et al. (2023): Frontal Polymerizations: From Chemical Perspectives to Macroscopic Properties and Applications. In: *Chemical Reviews* 123 (6), S. 3237–3298. DOI: 10.1021/acs.chemrev.2c00686.
5. Lang, Margit; Hirner, Stefan; Wiesbrock, Frank; Fuchs, Peter (2022): A Review on Modeling Cure Kinetics and Mechanisms of Photopolymerization. In: *Polymers* 14 (10), S. 2074. DOI: 10.3390/polym14102074.

Proceedings of the Composites 2024 International Conference
Seville, Spain – March 06 – 08, 2024
DOI: : https://doi.org/10.26799/cp-composites-2024

Development of feather-based materials

Krystyna Wrześniewska-Tosik, Tomasz Mik, Ewa Wesołowska, Tomasz Kowalewski, Michalina Pałczyńska, Justyna Wietecha
ŁUKASIEWICZ Research Network - Lodz Institute of Technology, Lodz, Poland, krystyna.wrzesniewska-tosik@lit.lukasiewicz.gov.pl

Abstract

This article explores the potential of feathers as a source of raw material for conversion into functional end-products such as nonwovens - geotextiles manufactured by the needling method to be used for agricultural sector. The composite feather-based material combines the characteristic of biodegradability with the ability to fertilize the soil during its biodegradation. This paper presents the characteristics of geotextiles made of feather and PLA/cotton by needle punch technique. The developed geotextiles were characterised in terms of mechanical properties such as thickness, strength, air permeability measurements ~~and~~ as well as biodegradation in soil.

Keywords: nonwoven, geotextiles, feathers, needle punch technique

1. Introduction

Geotextiles are widely used in agriculture, livestock, or earth-retaining structures [1]. Most of the nonwovens in use are made of synthetic fibres such as polypropylene (PP), polyester (PET), polyamide (PA), of which PP fibres account for 60% of all fibres used in the production of nonwoven fabrics [2]. According to a report by Global Market Insights, Inc. the size of the polypropylene nonwovens market was valued at USD 27 billion in 2019, in 2022 this value reached USD 41.7 billion and is expected to exceed USD 65 billion by 2032 [3]. All the above-mentioned fibres are characterized by a low susceptibility to biodegradation in natural conditions, which may result in environmental problems regarding soil contamination and accumulation of microplastics. The problem of the long decomposition cycle of such materials and the concern for the protection of the natural environment have in recent years resulted in significant interest in research and application of composite nonwoven fabrics containing fibres from natural or biodegradable polymers. Poultry feathers are a by-product of the poultry industry. The outstanding properties of feathers such as: hydrophobic properties, good thermal and acoustic insulation and biodegradability combined with their low cost and availability open way towards valuable and ecological products.

This paper presents the characteristics of geotextiles made of feather and PLA/cotton by needle punch technique. In general, the process starts with loosening of fibres, next the loose fibres are carded (combed) into a uniform web (fleece) constituting the carrier layer. Then the ground feathers are evenly fed to a single fleece running along the machine. Uniform web containing fibrous fleece together with feathers is lapped over itself several times to achieve a loose, continuous web of the desired density and weight. By combining individual webs, a multilayer composition is formed, which is then penetrated many times with barbed needles that push the upper layers of webs through the lower layers, thus interlocking them to achieve the thickness, strength and surface texture of the finished material. The penetration frequency and take-up speed are the factors determining the visual characteristics and strength of the nonwoven and can be easily modified to create desired products. To strengthen the multilayer nonwoven fabric, it is subjected to thermal consolidation using calendar or infrared heater at different temperature depending on the type of fibres used and the kind of consolidation.

2. Results

Technological trials for the manufacture of innovative, composite nonwovens by needle punching were carried out on an experimental line held by Łukasiewicz- Lodz Institute of Technology which is configured with the following devices: carding machine cutter, an aerodynamic moulding machine, fleece compacting rolls, a conveyor, a needle-punching machine and a coiler (Figure 1). Nonwoven were made of feathers with PLA /cotton. The question is: Why cotton? It was assumed that other cheap natural fibres would be introduced to reduce production costs. It was decided to replace some of the PLA with cotton waste (cotton waste generated during the production of various cosmetic products) and check how the addition of cotton would affect the biodegradation of the nonwoven fabric. ~~A~~ The method for producing these nonwovens was that the PLA /cotton were subjected to loosening and carding, after which they are arranged on a horizontal plane. In the next stage shredded feathers in the amount of up to 40 wt % was evenly distributed on such a single fleece. By combining individual layers, a multilayer composition was formed which was then subjected to a needling with take-up

DOI: : https://doi.org/10.26799/cp-composites-2024

1.5 -2.5 m/min, obtaining a multilayer nonwoven. To strengthen the multilayer nonwoven fabric, it was thermally consolidated using calendar.

Figure 1. Installation for producing nonwovens using needle punching method

It was investigated how different feather sizes affect the processing into nonwovens. Three feather sizes were used: < 0.125 mm; 0.125 -1.0 mm; 1.0 – 2.0 mm. The tables below present the composition of nonwovens and their mechanical properties. (Table 1, Table 2).

Table 1. Composition of nonwoven

Sample code	Feathers size, mm	Feathers content, %	PLA %	Cotton%
3 UN/23 „0”	-	0	50	50
3 UN/23	< 0.125 mm	30.0	35.0	35.0
4 UN/23	0.125 – 1.0	34.6	32.7	32.7
5 UN/23	1.0 – 2.0	29.0	35.5	35.5

Table 2. Mechanical properties of non-woven with feathers and PLA/Cotton

Sample code	Basis weight, g/m^2	Thickness, mm	Tensile strength in the longitudinal direction, N	Tensile strength in the vertical direction, N	Air permeability, l/m^2 s
3UN/23 „0”	102	1.85	8.87	21.0	1928,8
3UN/23	147	2.09	7.25	24.0	966,6
4UN/23	153	1.43	7.19	18.7	810,6
5UN/23	141	1.67	10.8	26.9	833,8

Samples of nonwovens were also subjected to biodegradation tests. The research objective of this study was to verify the influence of poultry feather addition on accelerating the biodegradation of nonwovens in cultivated soil [4]. The tests were carried out in laboratory conditions based on the assessment of weight loss. The biodegradability was conducted in soil under the controlled conditions of temperature (30 ± 2°C) and humidity (60-75%).). The incubation process was carried out for a maximum period of 24 weeks (Table 3)

Table 3. Biodegradation of nonwoven with feathers and PLA /cotton

Sample code	Biodegradation time -24 weeks Weight loss %
3UN/23”0”	52.6
3UN/23	67.6
4UN/23	70.8
5UN/23	59.6

DOI: : https://doi.org/10.26799/cp-composites-2024

Additionally, the ecotoxicity tests were conducted [5]. The main aim of the ecotoxicity tests was to investigate the influence of the nonwovens, with and without feathers addition, to the microbiological activity of the tested soil (Table 4).

Table 4. Results of microbiological tests (test environment: soil)

Weeks	Reference soil	Sample code		
		3UN/23	4UN/23	5UN/23
	Number of colonies *[Colony forming unit, CFU]*			
0	1.1×10^6	1.1×10^6	1.1×10^6	11×10^6
1	1.1×10^6	7.0×10^5	5.6×10^5	7.1×10^5
4	3.7×10^5	2.0×10^5	4.7×10^5	4.1×10^5
8	9.5×10^5	5.7×10^5	6.6×10^5	7.8×10^5
12	2.5×10^5	2.9×10^5	2.4×10^5	4.6×10^5
16	4.0×10^5	3.6×10^5	1.2×10^5	2.3×10^5
20	3.2×10^5	2.7×10^5	3.7×10^5	3.2×10^5
24	1.5×10^5	1.0×10^5	1.3×10^5	2.2×10^5

3. Conclusion

The addition of feathers does not significantly affect the mechanical parameters, only the air permeability decreases in relation to the sample without feathers.

The experiments confirmed the positive effect of the presence of feathers and cotton on the biodegradation of the tested materials. The level of mass loss after 24 weeks reached an average of 59-67.8 % for samples containing feathers with cotton, while nonwoven without feathers reached 1.51 % weight loss after 24 weeks. It can be assumed that the chemical compounds present in feathers (mainly keratin) have a positive effect on the activity of soil microorganisms, accelerating the biodegradation time of the whole sample.

Performed tests showed no toxic effect to the microorganisms, which was very important due to the essential role of microorganisms in the biodegradation process.

Acknowledgements

The investigation presented in this paper was carried out as a part of research project UNLOCK “Unlocking a feather bioeconomy for keratin-based agricultural products”. Grant Agreement number: 101023306 — UNLOCK — H2020-BBI-JTI-2020

References

1. C.W. Hsieh, “Geotextiles in agriculture and aquaculture”, in *Geotextiles From Design to Applications*, Woodhead Publishing, 2016, 511-530
2. S. Mukhopadhyay, “Natural and synthetic fibres for composite nonwovens”, in *Composite Nonwoven Materials: Structure, Properties and Applications*, D. Das and B. Pourdeyhimi Ed Woodhead Publishing, 2014, pp 20-29.
3. Global Market Insights, Inc (2023) Nonwoven Fabrics Market Size, https://www.gminsights.com/industry-analysis/ nonwoven-fabrics-market
4. Determination of the degree of decomposition of plastics and textiles in simulated soil conditions on a laboratory scale. Method of determining the loss of mass”(developed on the basis on international standards PN ISO 11266: 2020:11; PN-EN ISO 11721-1: 2002 and PN-EN ISO 11721-2: 2005).
5. Ecotoxicity- Test method: „Assessment of the influence of natural and synthetic materials on soil microflora„ (developed on the basis on international standards (EN ISO 7218:2008; EN ISO 11133 and EN ISO 11133:2014-07/A1; EN ISO 4833-1:2013-12, and EN ISO 19036:2020-04).